AIAA JOURNAL
Vol. 34, No. 7, July 1996

Comparison of Maximum Entropy Direct Simulation Monte Carlo Code with Flowfield Measurements

Michael A. Gallis* and John K. Harvey†
Imperial College of Science, Technology, and Medicine, London SW7 2BY, England, United Kingdom

Numerical results have been obtained with an axisymmetric direct simulation Monte Carlo code for the flowfield around a 70-deg spherically blunted cone. The results are compared with recently acquired experimental data on the density of the flowfield and the heat transfer and pressure distributions along the surface of the body. The test cases studied cover the flow of nitrogen and chemically reacting real air for a wide range of Knudsen numbers (0.0002–2.0) that extend from continuum to rarefied. The direct simulation Monte Carlo code used for the simulations employs the maximum entropy method for the modeling of energy exchange and reactions in chemically active flowfields and the generalized Borgnakke and Larsen method for the modeling of energy exchange in nonreacting ones.

Nomenclature

A = reference area of the 70-deg cone, πR_b^2, m^2
C_D = drag coefficient
C_h = heat transfer coefficient for a surface element
C_J = heat transfer coefficient
C_p = pressure coefficient for a surface element
D = global drag of the body, N
Kn = Knudsen number based on the mean free path for variable soft sphere molecules
Kn_0 = nominal Knudsen number of V3G cases
P = pressure on the body
p = pressure on a surface element, N/m^2
Q = global heat transfer to the body, J
$\dot{q}$ = heat transfer to a surface element, J
R = gas constant, J/(kgK)
R_b = base radius of the body, m
S_e = area of surface element, m^2
s = distance along the surface, m
T_0 = stagnation temperature, K
u = freestream velocity, m/s
λ = mean free path, m
μ_0 = viscosity, kg/ms
ρ = freestream density, kg/m^3

I. Introduction

ONE of the goals that future space vehicles will have to achieve is to operate at higher velocities that will result in shorter mission duration. Since aerobraking will almost certainly be used in these missions to reduce significantly the initial mass of the vehicle, higher cruising speeds will increase the impact of the entry in to the atmosphere. A compromise between the maximum cruising speed and the minimum duration of the mission must be defined. Aerobraking is expected to affect the heating rates both in front of the vehicle and in the wake area. To maximize the payload fraction, accurate prediction of the heat transfer is required, especially as this may be higher than experienced in earlier missions. The interaction of the wake area of the flowfield with the base of the vehicle affects the design of the payload compartment that will need thermal protection. Although the pressure is very low, the recirculation of high-temperature particles gives rise to significant heat transfer to the payload compartment.

Study of the flowfield of these vehicles has so far been restricted to computer simulations because reproduction of the high-speed entry conditions is particularly difficult in ground facilities. The need to simulate re-entry phenomena under conditions of thermodynamical and chemical nonequilibrium has led to a large number of theoretical models for chemical reactions and energy exchange. The validation of these models has so far been limited to comparison with other models because no reliable experimental data have existed.

In the search for the most appropriate method, comparison with experimental data and validation of these models is necessary so that interpolation and extrapolation of the numerical codes to new cases can be done with confidence. Several wind tunnels in the United States and Europe have recently been used for studies of the flowfields around a 70-deg spherically blunted cone. Recently, experimental work in the rarefied hypersonic regime has been performed at 1) V3G at DLR, German Aerospace Research Establishment, in Göttingen, Germany, 2) SR3, Centre National de la Richerche Scientifique (CNRS), in France, and 3) the large energy national shock tunnel (LENS) (Calspan) in the United States. These experiments cover a wide range of experimental techniques with different sophistication, and a variety of measurements have been obtained for surface and flow properties.

The purpose of this paper is to compare the predictions of the maximum entropy[1,2] direct simulation Monte Carlo (DSMC) code with the results of these experiments. All of the cases that have been simulated are for 0 deg of incidence.

II. DSMC Code Used

The particle solver used in this study is a DSMC axisymmetric code employing the variable soft sphere (VSS) model of Koura and Matsumoto.[3] The code uses structured multiregional mesh to achieve the best possible distribution of cells in the computational domain. Weighting factors are used in the radial direction to reduce the number of particles used in the simulation. The code simulates translational, rotational, vibrational, and electronic energy modes. Apart from the vibrational and the electronic energy modes that are treated in quantum states all of the others are treated as continuous distributions.

For the case of the chemically reacting flows a modification of the maximum entropy (ME) method,[1] first developed by Levine and Bernstein,[2] is used for the simulation of chemical reactions and energy exchange. The ME method does not use the equilibrium distributions for the simulation of the energy exchange process that have been the basis of the DSMC scheme so far, but it calculates the most probable distributions as deviations from a particular distribution. This makes the method particularly useful for the simulation of flows where significant degrees on nonequilibrium are experienced. The deviation of the postcollision energy distributions from the equilibrium one has found to be significant in almost all reactions. This

---

Received Feb. 10, 1995; revision received Aug. 28, 1995; accepted for publication Sept. 1, 1995.

*Research Associate, Department of Aeronautics. Member AIAA.

†Professor of Gas Dynamics, Department of Aeronautics. Member AIAA.

is particularly important for the vibrational mode where the largest deviations are met. The modification of the ME method by Gallis and Harvey,[1] used in this study, includes the effects of the molecular model that were missing from the original ME distributions. In the context of this method the deviation is expressed in the form of an exponential term that is simply added to the equilibrium distributions. In the model used in this study, the ME analysis was restricted to the vibrational mode because it presents the most significant variations from the equilibrium distributions. The same analysis could have been applied to the rotational mode, although it was considered unnecessary in this study.

For the calculation of the probability of chemical reactions, the principle of microscopic reversibility is used. This principle (see Levine and Bernstein[2]) requires that the same measure that describes the specificity in the energy disposal of the forward reaction described the energy selectivity of the reverse reaction. Using this principle, the Larsen–Borgnakke ME[1] analysis for the postcollision energy states can be repeated for the reacting energy states to formulate the chemical reaction probabilities. This means that exactly the same formulation that was used for the energy disposal can be used for the prediction of the probability of a chemical reaction. Depending on the type of the reaction (dissociation, exchange, or ionization reaction), the vibrational or the translational mode is used as a parameter controlling the reaction, as appropriate.

For the case of nonreaction collisions, the ME distributions reduce to the equilibrium distributions and the ME model becomes a generalized Borgnakke and Larsen type of model.[1] Our model employs a serial application of the Borgnakke and Larsen model to each of the energy modes involved in a collision. The rotational energy states are treated as a continuous distribution, whereas the vibrational states are treated as quantized energy states following the harmonic oscillator model. The rotational energy mode, therefore, is assumed to be distributed in the same serial manner according to the equilibrium distributions for all collisions, reactive or not.

For the simulations, a computational grid of approximately 9000–12,000 cells was used depending on the case. A representative case of a grid of 12,000 cells is presented in Fig. 1. This grid was used for the simulation of the SR3 case (see Sec. III.B). Similar grids were constructed for the other cases. The selection of the particular grids used in each case aimed at avoiding grid dependence problems in the results and was consistent with accepted practice within the DSMC community. Grid independence was achieved for almost all cases, apart from the second LENS case where the very high density close to the surface the computational grid did not seem to suffice (see the discussion in Sec. III.C). A more detailed consideration of the effects of grid resolution and the sensitivity of the results on the number of particles simulators is included in the Appendix.

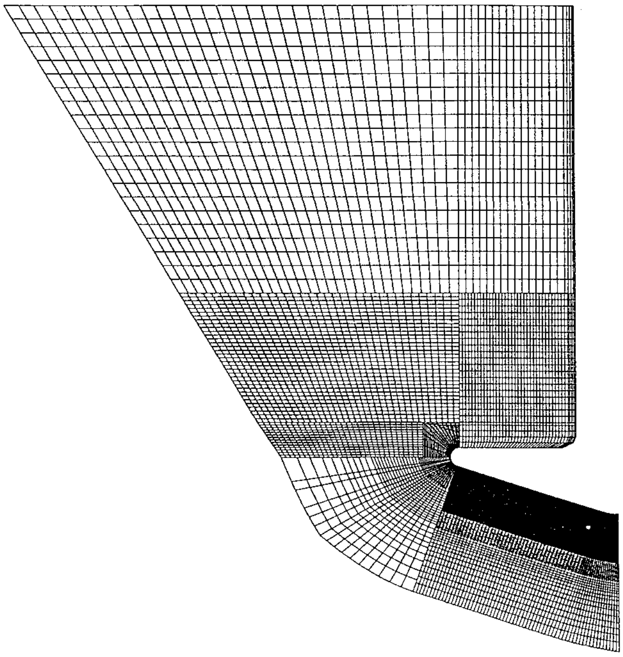

Fig. 1 Grid used for the SR3 case.

III. Simulation Results and Discussion

A. Simulation of the V3G Experiments

In the first set of experiments conducted by Legge,[4] the drag and heat transfer coefficients for the whole body were measured. The body used in the simulation was a 70-deg spherically blunted cone with a base diameter of 5 mm. The body was suspended in the wind tunnel by thin thermocouple leads without a sting. The heat transfer was measured, using the body as a calorimeter, concurrently with the forces that were recorded with a microbalance. The experiments were made for a Knudsen number ranging from 0.001 to 6 and they were repeated for 0, 20, and 40 deg of incidence. The experiments were conducted for two stagnation temperatures, $T_0 = 300$ K and $T_0 = 500$ K. The overall accuracy of the experiments was estimated to be ±8% for the 300 K case and ±12% for the 500 K cases. The Mach number for all cases was estimated to be 9.0048.

The results of the simulation for the heat transfer (C_H) and the drag (C_D) coefficients are shown in Figs. 2 and 3 in comparison with the experimental results. Open symbols have been used for the 300-K cases and closed ones for the 500-K cases to facilitate comparison between the predictions for the two different temperatures. In these figures the x axis is a function of a Knudsen number Kn_0 defined by Legge[4] as

$$Kn_0 = 3.2\frac{\mu_0}{\rho\sqrt{2\pi R T_0}\, 2R_b} \tag{1}$$

where μ_0 is the viscosity of nitrogen at the stagnation temperatures, equal to 0.223×10^{-4} kg/ms at 295 K and to 0.334×10^{-4} kg/ms

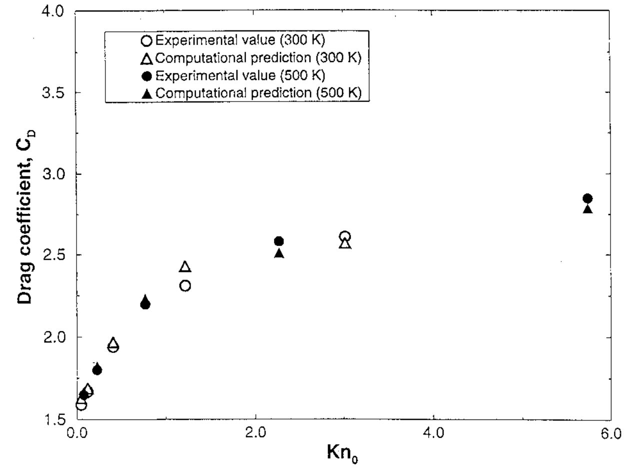

Fig. 2 V3G tests, C_H.

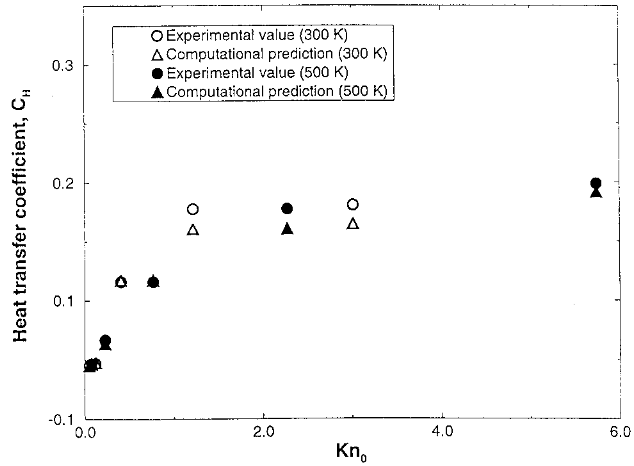

Fig. 3 V3G tests, C_D.

at 500 K. The heat transfer coefficient and the drag coefficient both in the experiments and in the code were calculated as

$$C_D = D\Big/\tfrac{1}{2}\rho u^2 A, \qquad C_H = Q\Big/\tfrac{1}{2}\rho u^3 A \tag{2}$$

The computational and experimental results are in good agreement for both temperatures and all Knudsen numbers. In all cases the discrepancy between the experimental and the calculated coefficients was found to be less than the experimental accuracy. For the heat transfer, the largest discrepancies in percentage are found in the least rarefied cases where the wall tends to be almost adiabatic. For the same cases, the drag coefficient presents a significantly smaller deviation from the measured value. The discrepancy of the small heat transfer coefficients is attributable to a large extent to the difficulties of measuring the heat transfer when small magnitudes are dealt with.

Because of the low temperatures at which this experiment was conducted, the vibrational energy mode was virtually unexcited. The simulations presented in Figs. 1 and 2 included the vibrational energy exchange, but calculations repeated with the vibrational mode completely suspended did not, as expected, show discernible differences. The energy exchange in these flowfields, therefore, was restricted to between the translational and the rotational mode.

The heat transfer and pressure coefficients are associated with the energy and momentum content of the flow. Their correct prediction in these cases validates the translational–rotational energy exchange used in the code and demonstrates convincingly the ability of the code to predict these coefficients. The agreement that was achieved between the measured and the calculated coefficients gives us the confidence to move on to more complex cases.

B. Simulation of the SR3 (CNRS) Experiments

The second set of comparisons corresponds to the conditions of the tests conducted by Allegere[5] in the SR3 tunnel at CNRS. The body tested was again the 70-deg spherically blunted cone but in this case it was supported by a sting. In these experiments the heat transfer and drag coefficients were measured along the surface of the body and the flowfield density was obtained using electron beam fluorescence.

Three different models were used, according to the type of measurements. For aerodynamic force measurements the model was made of aluminium and uncooled. It was directly mounted on the external balance housed around the open-jet test section of the SR3 wind tunnel. The model used for the flowfield density measurements was made of brass and was water cooled. For the heat flux measurements, thin elements made of Armco steel were embedded on the forebody, on the base surface, and around the cylindrical sting.

The Knudsen number for the SR3 cases varied from 0.001 to 0.032 and the Mach number from 20.0 to 20.5. The Knudsen number Kn is now and for the rest of this paper based on the mean free path λ that was determined for the VSS molecular model used in the simulations. In this paper one of these cases, the middle density one, will be simulated. The conditions of this case are given in Table 1.

For this simulation, a computational grid of 12,000 cells was used with 500,000 particle simulators. Most of the cells (around 10,000) were gathered in front of the body where the large densities are found. A total of 25,000 time steps was executed, assuming steady state after 15,000.

The nondimensionalized density profile for the flowfield is given in Fig. 4. The nondimensionalization has been done with the freestream density. In this figure the flow comes from the left to the right. In front of the body, a shock wave is formed that extends behind it, surrounding the wake area. Immediately behind the body and between $x/R_b = 0.4$–1.6, we have the formation of a low-density wake area. At about $x/R_b = 2$, there is a very diffuse recompression shock that increases the density. The interaction of the recompression wave with the sting supporting the body results in the formation of a region surrounding the sting where the density peaks to around 50% of the freestream density. In the radial direction, the density rises again due to the presence of the conical shock layer that surrounds the wake area.

Table 1 Conditions of the SR3 case

Mach number	20
Stagnation temp, K	1100
Stagnation pressure, bar	10
$Kn, \lambda/R_b$	0.022
Reynolds number, 1/cm	838

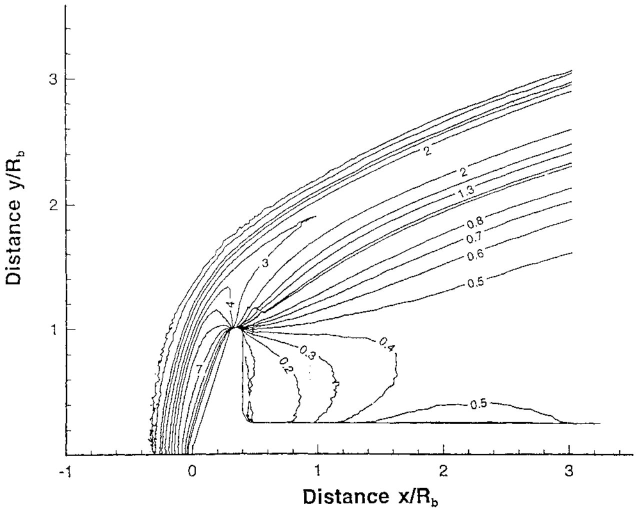

Fig. 4 SR3 test, nondimensionalized density profile, DSMC prediction.

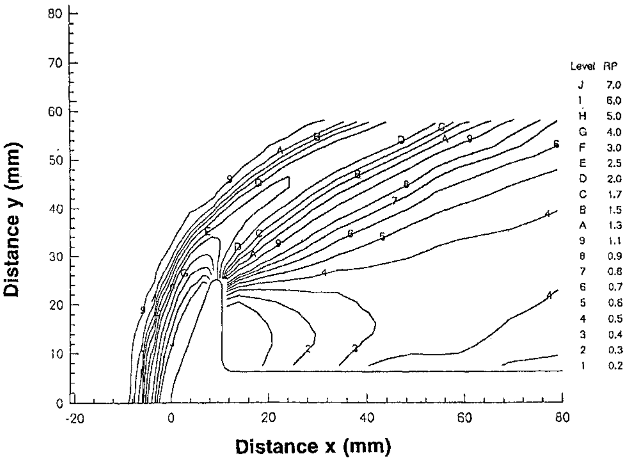

Fig. 5 SR3 test, nondimensionalized density profile, measured values.

Figure 5 presents the measured density profile.[6] We note that the measured and the calculated results are in excellent agreement, both in the low-density area behind the body and in the higher density in the shock wave. There is a small discrepancy of the results in front of the body in the low-density area (densities 1.05–2.00). Unfortunately, the experimental results have had to be corrected for slight flow nonuniformity, and they cannot be relied on to this degree in that area. As a result one cannot conclude whether this discrepancy is real or an artefact on the measuring technique.

The heat transfer on the surface of the vehicle as calculated with the DSMC code is presented in Fig. 6. The heat transfer coefficient has been calculated as

$$C_h = \dot{q}\Big/\tfrac{1}{2}\rho u^3 S_e \tag{3}$$

The horizontal s/R_b axis is the distance along the surface of the body from the stagnation point. In the same figure the measured values are given by solid circles. The maximum value of the heat transfer is found at the stagnation point. After a flat area that corresponds to the forebody area, the heat transfer presents a local peak that corresponds to the shoulder of the cone. After that the heat transfer drops by three orders of magnitude in the area that corresponds to the back of the body. This drop in the heat transfer is due to the rapid expansion around the outer rim of the body. The

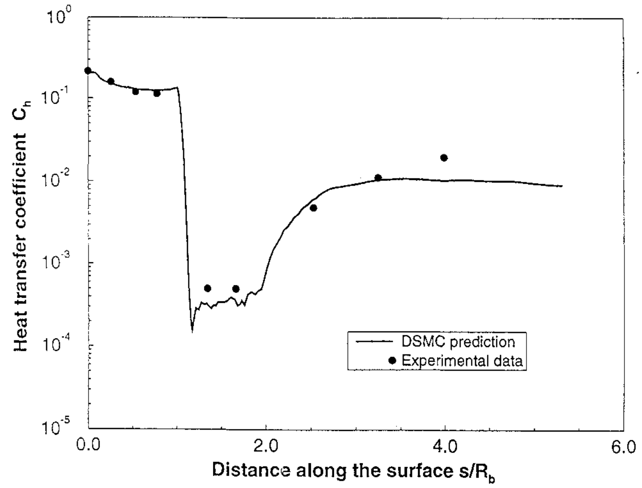

Fig. 6 SR3 test, nondimensionalized heat transfer coefficient.

measurements[7] behind the body (s/R_b = 1.1–2.0) gave the only indication that the heat transfer was less than the value indicated by the markers (0.0005). The heat transfer starts rising again along the sting of the body and finally reaches a plateau. This increase in the heat transfer along the sting is due to the reattachment and the interaction of the recompression wave with the sting in this area. The last measured point along the sting appears to be higher than the rest points of the plateau. This anomaly can be attributed to interaction of the suspension of the body because there is no physical reason for it to be there. Apart from this point, the calculated and measured results are in good agreement in all positions both in the forebody and along the sting. This result confirms the findings of the preceding section for the V3G results that the heat transfer to the vehicle can safely be predicted by the DSMC code.

Results for the same case have been published[8] indicating the same agreement as the one achieved here with a totally independently written code. Although this agreement could be expected, since the two codes used for the simulations used similar energy exchange models with the same relaxation parameters and similar grids, it is an encouraging result indicating the capabilities of the DSMC codes today.

The cases that have been presented so far have dealt with relatively large Knudsen numbers lying clearly in the rarefied regime. In the following examples the code will be extended to denser calculations lying in the transition and the continuum regime including one case that is chemically reacting.

C. LENS (Calspan) Experiments

The LENS[9] series of experiments are the highest enthalpy cases presented in this paper. The enthalpy of these flowfields allows extensive vibrational excitation, as well as dissociation of the gas mixture in some cases. The body that was simulated in this case is a 70-deg cone similar to the one used in the previous cases. The base radius of this model R_b was 3 in., and it was suspended by a sting with radius of 0.75 in. This case has been studied at zero angle of attack. In these experiments the heat transfer and pressure coefficients were measured along the surface of the body. Total temperature and pitot pressure were used to calibrate the flow. Freestream properties and concentration levels for the high enthalpy cases were computed from the known reservoir conditions.

The size of the LENS driver and driven tubes provide the capability to obtain test times up to 18 ms at velocities of 1500 m/s and 3–4 ms of uncontaminated time at 4800 m/s. These running times are necessary to study the effects of chemistry on the heat transfer on the vehicle for such flows comprising very dense and very rarefied regions. The main reason for the long flow establishment time is the recirculation region in the wake behind the body. The velocities in this area of the wake are small compared to the ones in front of the body that results in an increase of the time needed to reach steady state. In addition to the rarefaction of the flow, the occurrence of chemical reactions increases the time the flow needs to reach steady state.

Table 2 Conditions of LENS-B case, freestream gas conditions

Flow composition	N_2
Mach number	16.63
Density, kg/m^3	1.306×10^{-3}
Kn	4×10^{-3}
Pressure, psia	5.84×10^{-4}
Temperature, K	103
Wall temperature, K	295

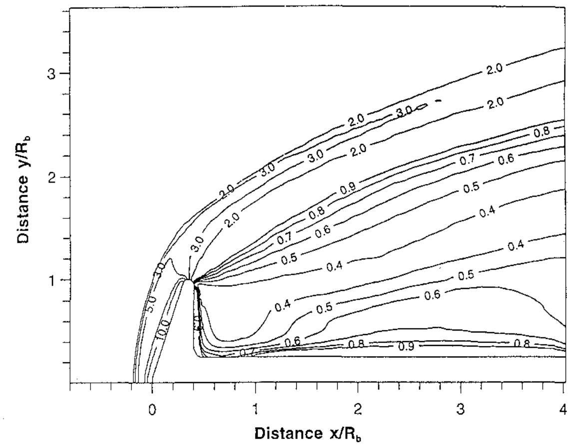

Fig. 7 LENS B case, nondimensionalized density profile.

Two cases will be simulated in this study. The first one is a nitrogen flow, and the second one is an N_2, O_2, NO, O mixture both at about Mach 15. The Knudsen number of the LENS cases is very small and that puts all of these cases well into the continuum regime. As a result, these cases are very demanding in computer time and resources. Particular care was exercised to make sure that grid resolution effects were avoided. The high enthalpy of these cases allowed vibrational excitation and dissociation of the molecular species of the flow.

1. LENS Case B: Nitrogen Flow

The first case corresponds to the flow of nitrogen at Mach 15.63 with a freestream temperature of 103 K and a freestream density of 1.306×10^{-4} corresponding to Knudsen number of 4×10^{-3}. The conditions of this case, the Calspan so-called case LENS-B (reservoir pressure 1000 psia), are summarized in Table 2.

The calculation was done with 500,000 particles over a grid of 12,000 cells, presented in Fig. 1. The nondimensionalized density profile for this case is shown in Fig. 7. All dimensions have been nondimensionalized with the vehicle base radius. In this figure the flow comes from the left to the right. The figure shows a high-density area adjacent to the cold wall of the body, where values above 100 times the freestream density are found. There is also a region of high density just behind the body that is created due to the recirculation of the particles in the area of the wake. Similar phenomena have been observed for similar cases by Moss et al.[8] and Gallis and Harvey.[10,11] On the sting at $x/R_b = 2$ there is a diffuse recompression wave that makes the density rise. In calculations without the sting an elliptic high-density region appears in the same position (see Ref. 10). Because of the sting, this elliptic area diffuses and covers a relatively larger area. Downstream of this area the density drops again. This denser region is where the flow recompression replaces the shock wave that would have been seen if the flow had been denser. The density profile was not measured in this experiment and so confirmation can be made that this diffuse recompression exists at predicted.

The heat transfer and pressure coefficients are presented in Figs. 8 and 9, respectively, in comparison with the experimental results. As is usual for rarefied flows the pressure coefficient in Fig. 9 has been defined as

$$C_p = P \Big/ \tfrac{1}{2}\rho u^2 \qquad (4)$$

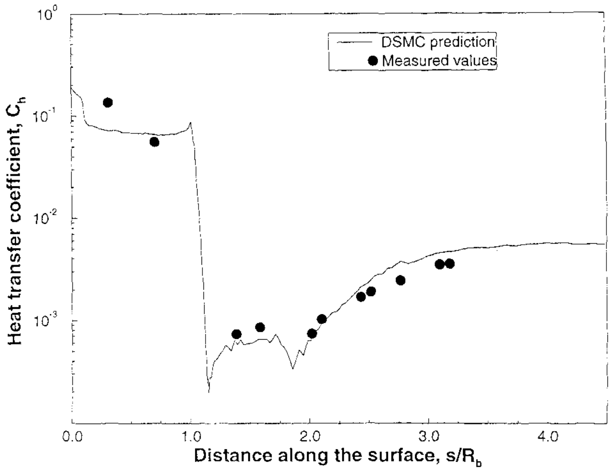

Fig. 8 LENS B case, heat transfer coefficient.

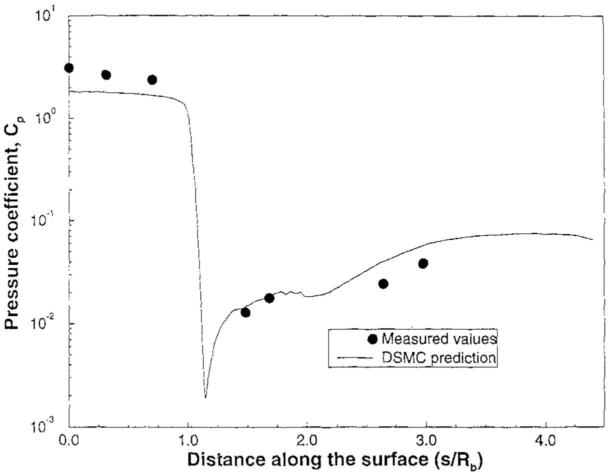

Fig. 9 LENS B case, pressure coefficient.

where P is the pressure of surface at a particular position. This enables a logarithmic representation to be used because C_p is always positive.

In a similar manner to the SR3 cases, the horizontal axis is the distance along the surface of the body from the stagnation point. Both the heat transfer and the pressure were found to peak at the stagnation point. Their behavior follows the pattern of the heat transfer coefficient presented for the SR3 case, and after a relatively flat area that corresponds to the front body, the heat transfer and pressure coefficient drop by three orders of magnitude on the back of the body. The experimental results are presented in the same figures with the solid circles marking measured values. We note that a generally good agreement has been achieved between the experimental and the computed results. The pressure coefficient seems to be overestimated in the area of the wake. At the same positions, the heat transfer coefficient appears to be in better agreement with the experimental results.

It is noteworthy that the heat transfer coefficient peaks locally in the area of the interaction between the base of the body and the sting to start rising again at about $s/R_b = 1.6$ along the sting. A similar phenomenon was found by Moss et al.[8] in their simulations for dense flows. This peak is due to the small localized vortex that is formed in this part of the flow. The higher velocities of the particles there increase the energy transfer to the body. Unlike the heat transfer for the rest of the flowfield in this area, heat is more effectively transferred due to the increased number of surface collisions. Simultaneously with the heat transfer, the pressure coefficient increases due to the added momentum transfer. The formation of this eddy and the resulting peak in the surface properties is characteristic of relatively dense flows. According to the calculations of Moss et al.[8] this phenomenon weakens as the density of the flow decreases. The case that was simulated here was denser than the cases simulated by Moss et al.,[8] which explains why this phenomenon was so marked. The heat transfer starts rising again at about $s/R_b = 1.6$ due to the relatively high density and temperature area that is found on the sting ($x/R_b = 1.0$–2.0). This makes the drag and heat transfer coefficients peak at roughly the same position. Evidently this peak is due to the higher energy content of the particles in this area.

Table 3 Conditions of LENS-C case, freestream gas conditions

Mole fraction N_2	0.7434
Mole fraction O_2	0.1668
Mole fraction O	0.001032
Mole fraction NO	0.08873
Mach number	10.31
Density, kg/m^3	4.315×10^{-3}
Kn	1.7×10^{-4}
Pressure, psia	0.039
Temperature, K	218
Wall temperature, K	295

2. *LENS Case C: Reacting Air*

The experimental effort towards studying the flowfield of blunted cones has been focused almost exclusively in nonreacting nitrogen flows. This has restricted the validation of numerical codes to simple flows lacking chemical activity. An exception to this rule is the Calspan LENS-C case that was conducted with high enthalpy simulated air. The enthalpy of the flow allows full excitation of the vibrational mode and a limited number of chemical reactions to take place (mostly exchange reactions and some oxygen dissociation). Again, the 70-deg blunted cone shape has been used, but the test gas was air at 3 km/s.

The conditions of the simulation, which is the highest enthalpy case and the highest density simulated in this paper, are given in Table 3. For the simulation of this case, 400,000 particle simulators were employed on a computational grid of approximately 12,000 cells. A total of 120,000 time steps was executed corresponding to 0.25 ms real flow time, and steady state sampling was initiated at 100,000 time steps.

The experimental results indicated that the time needed for the flow in the wake ultimately to reach steady state was about 3 ms. For the present calculation only a mere 0.25 ms time was simulated. The same time step was maintained throughout the flowfield making the solution time consistent but imposing at the same time a very significant overhead in the calculation. It is clear, therefore, that although the forebody flow must have converged, we cannot claim the same for the wake flow. The recirculation of the particles in the rarefied area of the wake increase the time needed for the flow to converge. It can be expected that within the time of this simulation the recirculation region in the wake should not have converged. An indication of this is that the reattachment point on the sting is closer to the back of the body than it should be.

Figure 10 shows the density and temperature profiles along the stagnation line. The flow comes from the left to the right. Far greater densities are found in front of the body than in the wake and the density reaches a value of above 100 times the freestream density next to the surface. Although the flow is rarefied, a distinct shock is produced at $x = -0.10R_b$ after which the density plateaus at the Rankine–Hugoniot value, and then rises smoothly, accelerating sharply near the surface. The backscattered particles that diffuse upstream cause the temperature to rise ahead to the density shock. The translational temperature starts rising at $x = -0.17R_b$ in what might be termed as thermal shock wave and reaches a peak of 23 times the freestream temperature and then gradually drops to roughly 20 times the freestream temperature. The rotational temperature lags behind the translational and starts rising at $x = -0.16R_b$, it reaches a maximum of 20 times the freestream temperature and then equilibrates with the other temperatures. The vibrational temperature starts rising at $x = -0.15R_b$ due to the chemical activity and equilibrates with the other temperatures at $x = -0.11R_b$.

The temperature in this part the flow allows a limited number of chemical reactions to occur. Above 4000 K (temperature achieved in the equilibrium region of the shock layer) partial oxygen dis-

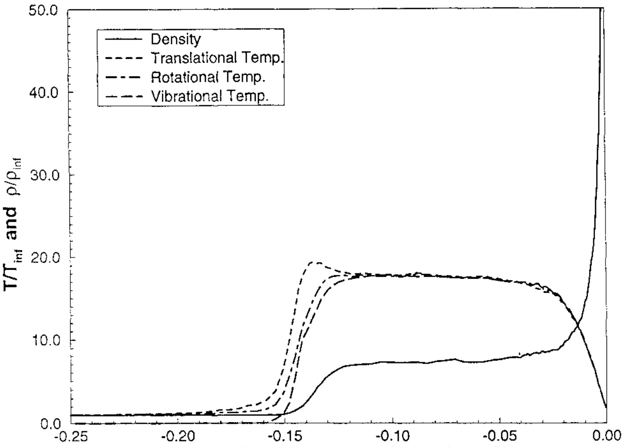

Fig. 10 LENS C case, stagnation streamline.

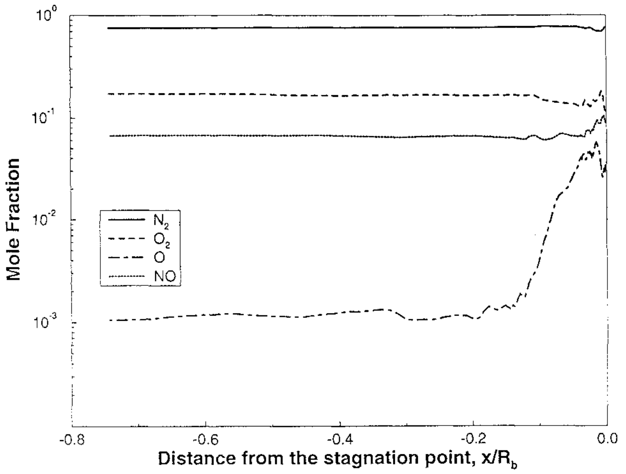

Fig. 11 LENS C case, species concentration along the stagnation streamline.

sociation takes place. Figure 11 giving the mole fractions of the species along the stagnation streamline shows that a very limited dissociation of the molecular oxygen, as well as some fluctuations in the fraction of NO. These fluctuations should be due to the exchange reactions taking place in this area of the flow. Exchange reactions take place between an atomic and a molecular species, and they usually have a very low or no energy threshold at all. Since a significant fraction of the flow is in atomic form, exchange reactions can be expected to take place. Because of the relative low temperatures met in the flowfield, direct dissociation of molecular nitrogen is not possible. It is interesting to note though that a very limited dissociation of molecular nitrogen takes place due to the $N_2 + O \rightarrow NO + N$ increases the concentration of NO and N at the expense of N_2. A maximum mole fraction of 10^{-5} of atomic nitrogen particles is achieved in the shock layer indicative of the extent that this reaction takes place.

The variation of the pressure coefficient along the surface of the probe is presented in Fig. 12 in comparison with the measured results. The calculated pressure coefficient peaks at the stagnation point at a value of about 1.84, and then after the flat region in front of the body, it rapidly drops to a very small value at the back of the body. In the wake area and along the sting where the densities start rising again due to the recompression wave, the pressure coefficient peaks again to 0.05 at $s = 3R_b$. After this peak and due to the expansion of the flow, the pressure coefficient drops again. Because of the large density difference between the forebody and the wake area, most of the particles of the simulation are gathered in front of the body leaving the very rarefied cells behind the cone nearly empty. As a result, no reliable prediction of the pressure coefficient in this area was obtained. In Fig. 12 the missing pressure coefficient values in the empty cells were linearly estimated from neighboring values.

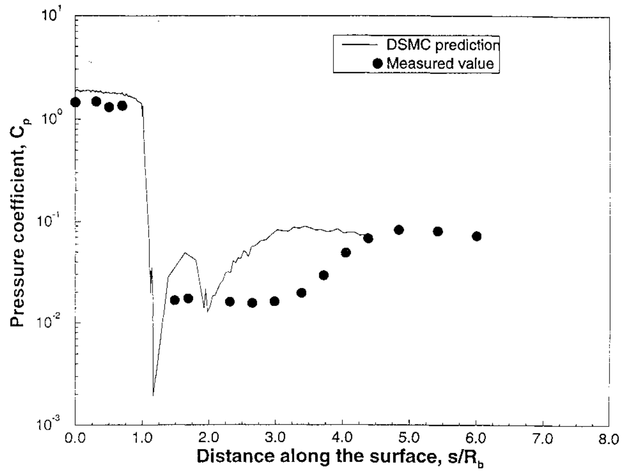

Fig. 12 LENS C case, pressure coefficient.

Although the pressure coefficient seems to be reasonably well predicted in front of the body, the comparison with the experimental results in the area of the wake is not as good as in the cases previously examined. Large discrepancies are seen between the measured and the calculated values for the two coefficients in the area of the wake. These discrepancies are due to the relatively short simulation time of the computation (0.25 ms). The time-dependent variation of the pressure coefficient in the wake obtained in the experiment indicated that the wake flow did not have the time to reach steady state before at least 3 ms of real time elapsed. Therefore, the discrepancy presented in Fig. 12 can be expected because not enough time for the flow to converge was simulated.

It should be noted here that in this case the classical convergence criterion of a maximum variation in the number of particles of less than 1% fails to capture the slow convergence rate of the flow. The number of particles in the flowfield appeared to have reached a steady state at 0.2 ms of real time flow, although the flowfield was far from convergent. In this case the very long relaxation times are due to the following two reasons.

1) Particles from the area around the stagnation point, where most of the chemical activity takes place, travel toward the rim of the body particles, conveying information to the wake about the chemical activity in the forebody area. The high density in the boundary layer makes them move with very small velocities and very high collision rate, this way slowing down in the passing of information.

2) The recirculation area behind the body further increases the time particles need to sweep the flowfield and to pass on flowfield information downstream. In the low-density area of the wake, collisions are very rare, and the only mechanism for passing information is the diffusion of particles.

It is almost impossible for any DSMC convergence criterion based on the number of particles to detect the steady state of this flowfield because the rate of change in the number of particles is smaller than the statistical error of the present simulation. A criterion this could be used to detect this slow convergence rate, however, would be observing the change in the heat transfer to the body. It should be pointed out, therefore, that convergence criteria in DSMC simulations cannot play a definitive role in the definition of the steady-state time, and the physical phenomena of the particular flow in question must also be considered.

In the forebody area, although the pressure coefficient is in reasonable agreement with the measured values, the heat transfer was found to be overestimated. This behavior, whereby the pressure is correctly modeled but the heat transfer is overestimated, is thought to be indicative of having insufficiently small computational cells adjacent to the body surface. These should be smaller than the local mean free path. The same behavior is repeated in the wake where the heat transfer was found to be overestimated. This should be attributed to the short simulation time, the effects of which were described in the previous paragraph.

The present calculation was made at a 32-bit workstation, and the use of smaller cells would have lead to numerical errors due to machine precision. It is anticipated that performing these calculations on a higher precision computer would have yielded better results for the forebody. The experimental evidence that the flow takes about 3 ms to reach steady state strongly suggests that the correct results for the wake can only be obtained if the simulation is run for long enough for this part of the flow to establish properly, allowing sufficient time for all chemical relaxation processes to take place, in addition to setting up the correct recirculation patterns. It is interesting to note that the conventional convergence criteria indicated that steady state was achieved earlier than it actually was. In the calculation of similar density cases, Gilmore[12] witnessed a significant change in the heat transfer coefficient from 0.3 to 1.1 ms of simulation time on the forebody, whereas the deviation in the number of particles was statistically insignificant. This observation indicates that the convergence of high density flows is not well understood yet, and special care ought to be exercised for their successful simulation.

IV. Conclusions

Comparison of the ME-DSMC code with experimental data is very encouraging, and it indicates that the code can be used as a reliable tool for the prediction of flowfields in the rarefied hypersonic regime, including wake and reattachment flows. Knudsen numbers down to 10^{-3} were successfully simulated giving accurate predictions for both the surface fluxes and flowfield characteristics.

Application of the code of the only test case for which chemical reactions took place within the flow was disappointing. The flow was well into the continuum regime ($Kn = 0.0002$), and it was a very demanding test case to attempt. Although the forebody pressure was modeled accurately, the heat transfer was overpredicted, probably due to lack of numerical resolution in the very small cells needed adjacent to the surface. The wake flow and reattachment on the sting was not modeled correctly. Experimental evidence on the wake flow establishment time gives a clear explanation for the failure. Although the DSMC calculation appeared to have reached steady-state solution, in real time this was about an order of magnitude less than the true time needed for the relaxation process, including processes associated with the chemistry to be completed behind the body. The cause for the failure is thus not inherent within the DSMC code but due to an inappropriate application of it.

Appendix: Effect of Grid Variations and Number of Particle Simulators on Computed Results

The importance of cell size in DSMC codes for the prediction of flowfield and surface properties has been the subject of extensive investigation. Bird[13] and Moss et al.[8] suggest that if the cell size is of the order of one-third of the local mean free path, then the results will be grid resolved. In many applications it is possible to choose cell patterns that are approximately aligned with the directions of steepest gradients of flow properties. In this case it has been shown that the requirement to have cell sizes less than one-third of the local mean free path can be relaxed along the direction of the flow. The requirement can also be relaxed for the freestream cells where no gradients are found. The prediction of surface flux properties has been found to be especially sensitive to the grid resolution in the vicinity of the surface. For the selection of the final grids used in the simulations, several preliminary ones were used until convergence was achieved, and the rules for the selection of the grids set by Moss et al.[8] have been confirmed and followed.

The DSMC code used in this study uses rectangular multiregional grids similar to the one used by Moss et al.[8] for the same body shape. Following their investigation a computational grid of 12,000 cells was found to suffice for these calculations, and this is what was used in the present study. Trial calculations were executed with a grid of 10,000 cells, and of particular importance, with coarser cells closer to the body, and no significant variations in the surface heat transfer were detected. These parameters have been found to be extremely sensitive indicators of cell size independence and code convergence.

The accuracy of the flowfield predictions in DSMC calculations is mostly influenced by the instantaneous number of particle simulators. To enhance the accuracy of the results and to reduce the statistical error, twice the number of particles was used compared to Moss et al.[8]; i.e., 500,000 were used in the present calculation compared to 200,000 by Moss et al.[8]

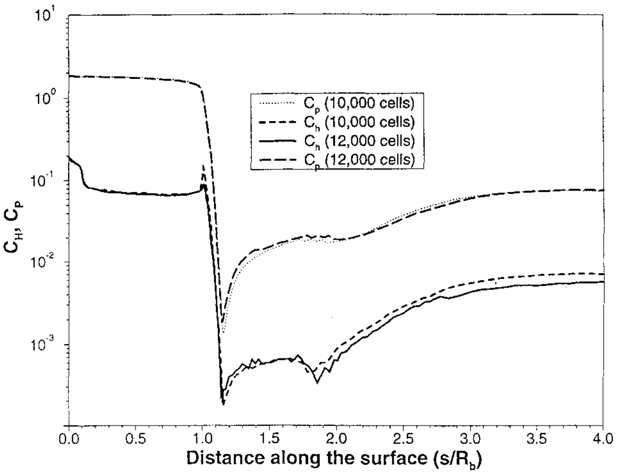

Fig. A1 Comparison of heat transfer and pressure coefficients for two grids for the LENS-B case.

The requirements of the LENS case B was found to be very similar to that of the SR3 case since the Knudsen numbers are similar. Again, a grid of 12,000 was used, but in this case the cells were weighted close to the surface to make sure that in the normal direction the third of the mean free path condition was satisfied. This alone should guarantee cell independence of the computed results, but to ensure this a trial calculation with 10,000 cells and 200,000 particles was made. Again in this case, no significant differences were found, proving that satisfaction of the third of the mean free path is enough to guarantee cell independence. A comparison between the heat transfer and pressure coefficients of the 12,000 and the less favorably distributed 10,000 cell mesh is given in Fig. A1. We note that the predictions are in very good agreement and do not appear to be affected by the number of cells employed.

The V3G cases covered a very wide range of Knudsen numbers (from 0.001 to 6), and the grids used changed to follow the requirements of each case. The grids used for these cases had the same structure as the one presented in Fig. 1 (without the wake) but with a varying number of cells. For the dense cases the same grids already described were used, whereas for the medium and large Knudsen numbers, the grid resolution was kept high by reducing the computational time step. Although this option resulted in longer execution times, it also ensured the grid independence of the results. In these cases, the number of particle simulators was kept constant at about 350,000 particles.

Steady state in the evolution of each solution was assumed to have been achieved when the fluctuations in the total number of particles fell below 1% for a period of several hundred samples (typically, over 1000 time steps). Experience has shown that this criterion is a simple way of confirming when the density throughout the flow has reached a steady state. At this point in time, sampling of flowfield properties was initiated, and the values averaged until a statistically acceptable smooth sample was achieved. None of the data presented in this paper have been smoothed in any way, and the low level of statistical noise is a good indicator of the level of convergence that has been achieved.

An exception to the described cell resolution rules was the LENS-C case. In this case the computational grid failed to satisfy the cell resolution requirements due to the very high densities that were met in the boundary layer, as explained in Sec. III.C. This was manifested with the prediction of high heat transfer to the surface. The flowfield for the LENS-C case was the only one here for which chemical reactions took place, and a more detailed study of the localized number densities was used to judge the beginning of the steady state, as described in Sec. III.C.

References

[1] Gallis, M. A., and Harvey, J. K., "The Borgnakke and Larsen Distributions as Prior Distributions in the Maximum Entropy Method," *Rar-*

efied Gas Dynamics, 19, Oxford Univ. Press, Oxford, England, UK, 1995, pp. 507–513.

[2] Levine, R. D., and Bernstein, R. B., *Molecular Reaction Dynamics and Chemical Reactivity*, Oxford Univ. Press, Oxford, England, UK, 1987.

[3] Koura, and Matsumoto, "Variable Soft Sphere Molecular Model for Inverse-Power-Law or Lenard Jones Potential," *Physics of Fluids A*, Vol. 3, No. 10, 1991.

[4] Legge, H., "Heat Transfer and Forces on a Blunted Half Angle Cone Measured in Hypersonic Free Jet Flow," DLR, German Aerospace Research Establishment, IB 222-93 A 33, Göttingen, Germany, Nov. 1994.

[5] Allegre, J., "The SR3 Low-Density-Tunnel; Facility Capabilities and Research Development," AIAA Paper 92-3972, July 1992.

[6] Allegre, J., and Bisch, D., "Experimental Density Flowfields over a 70° Blunted Cone at Rarefied Hypersonic Conditions," Fourth European High Velocity Database Workshop, European Space and Technology Center, Noordwijk, The Netherlands, Nov. 1994.

[7] Allegre, J., and Bisch, D., "Heat Transfer Measurements over a 70° Blunted Cone at Rarefied Hypersonic Conditions," Fourth European High Velocity Database Workshop, European Space and Technology Center, Noordwijk, The Netherlands, Nov. 1994.

[8] Moss, J. N., Dogra, V. K., and Wilmoth, R. G., "DSMC Simulations of Mach 20 Nitrogen Flows About a 70° Blunted Cone and Its Wake," NASA TM 107762, Aug. 1993.

[9] Holden, M. S., "Development and Code Evaluation Studies in Hypersonic Flows in the LENS Facility," Second European Symposium on Aerothermodynamics for Space Vehicles, European Space and Technology Center, Noordwijk, The Netherlands, Nov. 1994.

[10] Gallis, M. A., and Harvey, J. K., "Validation of DSMC Computations for the Flowfield Around Blunted Cones," *Rarefied Gas Dynamics*, 19, Oxford Univ. Press, Oxford, England, UK, 1995, pp. 1284–1290.

[11] Gallis, M. A., and Harvey, J. K., "Simulation of Chemically Reacting Flowfields Around a 70-deg Spherically Blunted Cone," *Journal of Spacecraft and Rockets*, Vol. 34, No. 4, 1995, pp. 581–587.

[12] Gilmore, M. R., "Rarefied Flow over a Blunt Body," British Ministry of Defence, Defence Research Agency Rept. DRA/DWS/WX7/TR 95-189, Feb. 1995.

[13] Bird, G. A., *Molecular Gas Dynamics and the Direct Simulation of Gas Flows*, Clarendon, Oxford, England, UK, 1994.